Automatic Welding Seam Tracking and Identification

Xinde Li, *Senior Member, IEEE*, Xianghui Li, Shuzhi Sam Ge, *Fellow, IEEE*, Mohammad Omar Khyam, and Chaomin Luo, *Member, IEEE*

Abstract—In the automatic welding process on mid/thick plates, the precision of the welding position has an important effect on welding quality, which mainly relies on the identification of the welding seam. However, due to some possible disturbances in complex unstructured welding environments, e.g., strong arc lights, welding splashes, thermal-induced deformations, etc., it is a great challenge to identify the welding seam. In this paper, we propose a robust automatic welding seam identification and tracking method by utilizing structured-light vision. First, after the preprocessing of the welding image, the gray distribution of the laser stripe is tracked and the profile of the welding seam is searched in a small area by using the Kalman filter, with the aim to avoid some disturbances. Second, in order to extract the welding seam profile, a series of centroids obtained by scanning the columns in the rectangular window are fitted using the least-squares method. Third, a character string method is proposed to qualitatively describe the welding seam profile, which might consist of different segment and junction relationship elements. And then, these character strings acquired from the object image are matched with those from the model, so that the position of the welding seam can be determined. Finally, the advantages of the new algorithm are testified and compared through several experiments.

X. Li is with the Department of Electrical and Computer Engineering, National University of Singapore, Singapore 117580, and also with the Key Laboratory of Measurement and Control of CSE, Ministry of Education, School of Automation, Southeast University, Nanjing 210096, China (e-mail: xindeli@seu.edu.cn).

X. Li is with the Key Laboratory of Measurement and Control of CSE, Ministry of Education, School of Automation, Southeast University, Nanjing 210096, China (e-mail: 230149424@seu.edu.cn).

S. S. Ge is with the Social Robotics Laboratory, Department of Electrical and Computer Engineering, Interactive Digital Media Institute, National University of Singapore, Singapore 117576 (e-mail: samge@nus.edu.sg).

M. O. Khyam is with the Faculty of Engineering, Department of Electrical and Computer Engineering, National University of Singapore, Singapore 117580 (e-mail: fahad_ete@yahoo.com).

C. Luo is with the Advanced Mobility Laboratory, Department of Electrical and Computer Engineering, University of Detroit Mercy, Detroit, MI 48221 USA (e-mail: luoch@udmercy.edu).

Color versions of one or more of the figures in this paper are available online at http://ieeexplore.ieee.org.

Digital Object Identifier 10.1109/TIE.2017.2694399

Index Terms—Automatic welding, Kalman filter, qualitative description, welding seam identification, welding tracking.

I. INTRODUCTION

INDUSTRIAL welding plays a very important role in the manufacturing process. However, due to the severe working environment and condition, few people prefer to choose it as a career, so that the shortage of skilled welding workers might make it necessary to develop a welding robot to replace the welding labors. In the past, industrial arc-welding robots were operated by teaching-programing of human operators, which took a great amount of time and expense to program paths and redefined welding parameters for each new part. Therefore, although a teaching-programing welding robot is more fit for the volume production task, it is difficult to afford the flexible one. Automatic welding [1], [2] is becoming increasingly popular in modern manufacturing and leading the revolution in welding industry, as it can intelligently run flexible production lines by online sensing [3], self-learning, and autorecognition.

However, in the process of automatic welding, welding seam identification is regarded as the basement of the welding seam tracking and welding gun positioning, the switch of welding mode, 3-D reconstruction of joint/groove, welding quality control, etc. Up to now, there are lots of welding seam identification methods for different types of joint/groove modes. For example, aiming at the V type of joint [4], some points of discontinuity on the welding joint profile were regarded as very distinct and invariable pattern features. However, the points of discontinuity acquired by analyzing the curvatures of line segments were very sensitive to noise for second derivative characteristics. In addition, they can yet not be regarded as the pattern features of some types of joints, i.e., lap joint, butt joint, etc. In order to overcome the shortcoming of the method in [4], Li *et al.* had a deep study on the V groove, direct butt joint without groove, and lap joint, where the main lines and points of discontinuity picked up from the laser stripe were regarded as pattern features [5]. Although the antinoise ability of these features had been greatly improved for special joints, the method was very sensitive to joint deformation, for example, the V type of groove might be deformed due to the assembly error in Fig. 1(a), the spot welding at the bottom of the groove used for fixing the workpieces before formal welding in Fig. 1(b), and the welding workholders on the two sides of the V type of groove in Fig. 1(c).
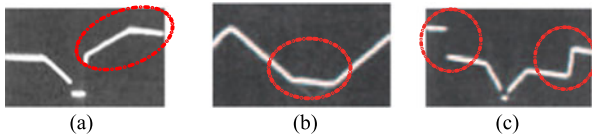
Fig. 1. Several kinds of V grooves deformed.

In [6], Sicard and Levine developed a string representation and recognition method for classifying three different types of joints detected by laser scanner,[1] i.e., butt joint, lap joint, and V joint. However, this method has low precision of the system if used in the structured-light vision, since it only considers the filter of profile points detected by a laser scanner, instead of considering an effective way to avoid the disturbances of noise in the welding image. In [7], the fillet welding joint was identified regardless of the base material, surface finish, and surface imperfections such as scratches, mill scale and rust, and an adaptive line-growing algorithm for robust identification was introduced without prior knowledge of the shape or position of the joint in the image. Also, in order to identify the narrow welding seams of various shapes and sizes for ferrous materials [8], a new method was also developed to combine with reliable image matching and triangulation through the use of 2-D homography. The advantage of this method was that, even in the presence of imperfections on the surface of steel, the seam could also be identified from a single image without prior knowledge of its geometry or location. However, sometimes, it was difficult to estimate the homography transformation using RANdom SAmple Consensus (RANSAC) [9]. In [10], an autonomous welding seam recognition algorithm was proposed, in which a pair of parallel welding seam edges were found in local area, and then, the remnant edge by iterative edge detection and edge linking by a shift window were searched from the two endpoints of each edge. However, the method might be invalid when the reflection of a work piece was very strong. The same team also presented a method for autonomously detecting welding seam profiles from a molten pool background in metal active gas (MAG) arc welding using a novel model of saliency-based visual attention [11]. In [12], arc, visual, and sound sensors were simultaneously utilized to obtain the electrical, sound, and welding pool image information of pulsed gas tungsten arc weld process, which were fused by the Dempster–Shafer rule [13]. Although this method is very robust for welding seam recognition, its cost for integrating three different kinds of sensors is very high [14]. In [15], in order to overcome the shortcoming of an arc-sensing-based method, the vision-sensing data were integrated into it using the support vector machine to predict the groove state.

A multiple-peak algorithm to detect laser profile is proposed for circular pressure vessel welding with a gantry welding robot to overcome the interference in a high-strength reflection area [16]. In [17], in order to pick up the profile of the laser stripe acquired from gas metal arc welding, a modified Hough
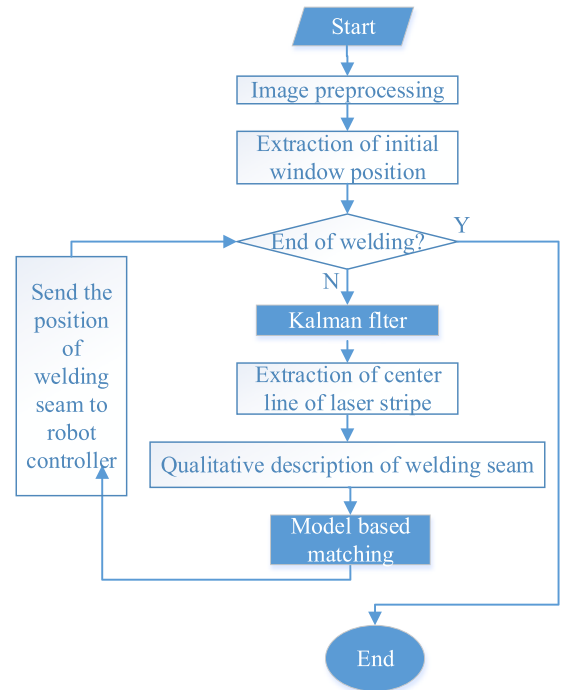

Fig. 2. Flowchart of the proposed method.

transformation algorithm was applied for the seam tracking system, which seemed very time-consuming for line detection.

In this work, a novel welding seam tracking and identification method with high efficiency, good precision, and strong robustness is proposed. Its main aims are: first, to try to avoid some disturbances caused by noise, reflections, etc., and search the profile of the laser stripe in a sufficiently small area using the Kalman filter, and second, to increase the robustness of the matching of the profiles from the object image and model by proposing a character string description and matching method. The whole flowchart of the new method is given in Fig. 2, which will be explained with details in the later sections.

This paper is organized as follows. In Section II, a type of structured-light vision model is established, in which the camera acquires the laser stripe to recognize the profile of the welding seam according to the measurement principle of triangulation. Section III presents a tracking algorithm based on the Kalman filter for tracking and searching for the laser stripe in a sufficiently small area of the object image. Section IV proposes a qualitative description method for explaining the profile of the welding seam, which is very robust in terms of integrating segment elements and recovering relationship elements. In Section V, several experiments are conducted to testify the static and dynamic precision and real-time performance of our new method by comparing with other methods. A conclusion drawn from this study is discussed in Section VI.

II. STRUCTURED-LIGHT VISION MODEL

A structured-light vision sensor system [18] is mainly composed of the camera, laser, optical filter, and dimmer glass.
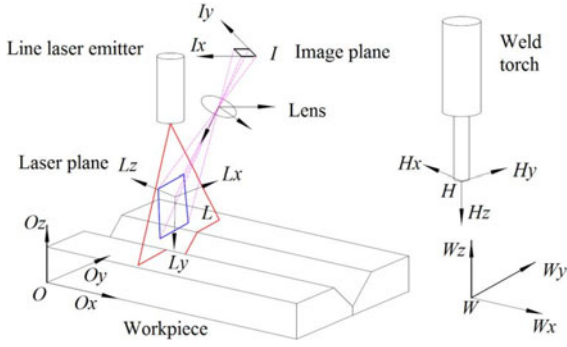
---

[1]Here refers to laser sensor different from the structured-light vision sensor, from which a scanning beam of light is transmitted across the joint, so that the welding seam profile is directly obtained from the recorded depth values.

Fig. 3. Structured-light vision model.

Fig. 4. Preprocessing result for the original welding image (a): (b) is the effect after step 1; (c) is the effect after step 2.

Of course, with the purpose of reducing the size of the sensor system, the reflective mirror is also fixed on it. The world coordinate system W, the workpiece coordinate system O, the welding gun coordinate system H, the camera coordinate system C, and the image coordinate system I are shown in Fig. 3, where the pose $_C^H T$ of the camera coordinate system in the welding gun coordinate system can be obtained through eye–hand calibration. The pose of the structured-light plane in the camera coordinate system C is also relative fixed, which may be described as $a^C x + b^C y + c^C z + d = 0$; here, the parameters $[a, b, c, d]$ can be calibrated through the structured-light, since the key of the structured-light imaging lies in the intersection relation between the laser plane and workpiece surface. Therefore, it is necessary to set up the laser coordination system L in the laser plane. Suppose the point of intersection between the optic axis of camera and the laser plane is the origin $^C o_L = (0, 0, -d/c)^{\mathrm{T}}$ of L. The z-axis of L is normal to the laser plane, whose vector is $^C \vec{z}_L = (a, b, c)^{\mathrm{T}}$. The x-axis of L is the projection of the x-axis of the coordinate system C to laser plane along the optic axis, i.e., $^C \vec{x}_L = (1, 0, -a/c)^{\mathrm{T}}$. The y-axis of L is obtained through the right-hand rule, i.e., $^C \vec{y}_L = {}^C \vec{z}_L \times {}^C \vec{x}_L = (-ab/c, c + a^2/c, -b)$. Furthermore, we get a normalized unit vector of every axis, i.e., $^C \vec{x}_L'$, $^C \vec{y}_L'$, and $^C \vec{z}_L'$, and the relation between the coordinate system L and C is $_L^C T = (^C \vec{x}_L', {}^C \vec{y}_L', {}^C \vec{z}_L', {}^C o_L)$. Therefore, the homography between the image coordinate system and the laser coordinate system is as follows:

$$ s \begin{bmatrix} I_u \\ I_v \\ 1 \end{bmatrix} = T_{\mathrm{hom}} \begin{bmatrix} L_x \\ L_y \\ 1 \end{bmatrix} \qquad (1) $$

where s is a scale factor and T_{hom} is homography.

III. KALMAN-FILTER-BASED TRACKING ALGORITHM

Although the optical filter and dimmer glass are installed at the structured-light vision sensor, some disturbances, e.g., splashes, reflections, etc., still are kept on the welding image, which might have a very severe effect on the extraction of profile, as shown in Fig. 4. Therefore, it is very necessary to avoid disturbances by reducing the search range of the laser stripe in the real welding image. That is to say, a laser stripe does not need to be searched in the whole image, but within the most
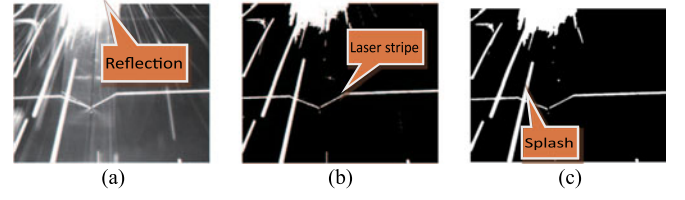
likely contained area. Of course, the position of a laser stripe might be variable in the different welding image frame, so that the position of the search window also follows its change. In order to obtain the window position O_{SW_k} of the kth frame of the image, we need to predict the window position $O_{\mathrm{SW}_{k/k-1}}$ using the Kalman filter [19].

A. Image Preprocessing

Since one welding image always suffers from the influences of optical noise, i.e., splashes, reflection, etc., a preprocessing step is carried out for the original image to reduce its effects as far as possible, in which the median filter algorithm is applied twice.

Step 1: The median filter algorithm is used for each column, in order to remove the noise with low gray in the original welding image. For example, the preprocessing effect of the original welding image in Fig. 4(a) after Step 1 is shown in Fig. 4(b).

Step 2: A 5×5 window is used in the median filter algorithm, in order to remove a little noise with high gray in the image. For example, the preprocessing effect of the original welding image in Fig. 4(a) after Step 2 is shown in Fig. 4(c).

B. Extraction of the Initial Window Position

Since the window position in the current frame may be predicted through the previous frame, the accuracy of the window position in the first frame is very key. With the aim to adaptively pick up the initial window position, the center line of the laser stripe is extracted by scanning the gray column by column in terms of the center-of-gravity method [20]. The position coordinate of the center line is given as follows:

$$ \begin{cases} p_i(x) = i \\ p_i(y) = \sum_{\nu=j}^{k} \frac{g(i,\nu) * \nu}{\sum_{\nu=j}^{k} g(i,\nu)} \end{cases} \qquad (2) $$

where $p_i(x)$ and $p_i(y)$ represent the coordinate of the point p_i on the center line. ν is the y coordinate of the pixel on the stripe line, i.e., $\nu \in [j, k]$, and j and k are the y coordinates of the bottom and top of the stripe. $g(x, y)$ is the gray of pixel (x, y). The center line consists of points p_i extracted, which is expressed as $P = \{p_i\}, i = 1, \ldots, M$.

Since the position of the laser stripe in the monitoring field of the structured-light vision sensor might be changeable with the motion of the welding gun, the size of a search window becomes very important. That is to say, if larger a search window becomes, more time it will take to search; moreover, more noise there might be including in the window. However, if smaller

the size of window becomes, more likely the stripe is out of window. Therefore, the initial rectangular window is defined by its four vertexes as

$$\begin{cases} X_l = \min(p_i(x)), & i = 1, \ldots, M \\ X_r = \max(p_i(x)), & i = 1, \ldots, M \\ Y_t = \min(p_i(y)) - \alpha \times \Psi, & i = 1, \ldots, M \\ Y_b = \max(p_i(y)) + \alpha \times \Psi, & i = 1, \ldots, M \end{cases} \quad (3)$$

where X_l, X_r, Y_t, and Y_b are the four vertexes (left, right, top, and bottom) of the rectangular search window, respectively. Ψ is the width of laser stripe. α is the proportional factor of laser stripe.

C. Prediction of the Position of the Window

Since the position of the search window might suffer from disturbances of the noise, e.g., welding splashes, reflections, sensor or welding gun motion, and so on, which might be changeable in different frames of images, it need to be estimated with the Kalman filter [2] here.

Known the observation sequence Z_k of the position of the search window, in order to obtain the linear minimum variance estimation O_{SW_k} of the system state $O_{SW_{k/k}}$, we need to predict the most likely position $O_{SW_{k/k-1}}$ in the kth frame of the welding image, in terms of the position $O_{SW_{k-1/k-1}}$ of search window in the $(k-1)$th frame of the image, integrating with the motion state information

$$O_{SW_{k|k-1}} = A \times O_{SW_{k-1|k-1}} + W_k \quad (4)$$

where A is the system parameter and W_k is the generated random noise of the system at time k. And then, the corresponding covariance $P_{k/k-1}$ is derived as follows:

$$P_{k|k-1} = A \times P_{k-1|k-1} A^T + Q \quad (5)$$

where $P_{k-1/k-1}$ is the corresponding covariance of the position $O_{SW_{k-1/k-1}}$, and Q is the covariance of the random noise W_k in the course of system motion.

And then, after the preprocessing of the kth frame of the image, a measurement of position Z_k of the search window is carried out. Therefore, we can obtain the filter correction value of the kth frame as follows:

$$V_k = Z_k - H \times O_{SW_{k|k-1}} \quad (6)$$

where H is the measurement parameter. Finally, we can calculate the position $O_{SW_{k|k}}$ of the search window according to the prediction value $O_{SW_{k/k-1}}$ and the correction value V_k:

$$O_{SW_{k|k}} = O_{SW_{k|k-1}} + Kg_k \times V_k \quad (7)$$

where Kg_k is the filter gain of the kth frame of the image, which is derived as follows:

$$Kg_k = \frac{P_{k|k-1} \times H^T}{\left(H \times P_{k|k-1} \times H^T + R \right)} \quad (8)$$

Algorithm 1: Algorithm of the Kalman filter.

Input: $O_{SW_{k-1/k-1}}, P_{k-1/k-1}$, and the kth frame of the welding image.

Output: $O_{SW_{k/k}}, P_{k/k}$.

1) *The extraction of initial window position.*
   * Calculate the initial position sequences $P = \{p_i\}, i = 1, \ldots, M$ of center line by scanning column by column according to (2).
   * Compute the initial position $(x_{\text{center}}, y_{\text{center}})$, width, and height of the search window in terms of (3)
   * $k = 1$.

2) *While input == true*
   * Calculate the position $O_{SW_{k|k-1}}$ and its covariance $P_{k/k-1}$ of the search window in the kth frame of the image utilizing (4) and (5).
   * Preprocess the kth frame of the image.
   * Measure the position Z_k of the search window.
   * Compute V_k using (6).
   * Compute Kg_k using (8).
   * Compute $O_{SW_{k/k}}$ using (7) and update its covariance $P_{k/k}$ utilizing (9).
   * $k = k + 1$.
   * End.

---

where R is the variance of V_k. The covariance $P_{k/k}$ of $O_{SK_{k/k}}$ is updated as

$$P_{k|k} = (I - Kg_k \times H) \times P_{k|k-1}. \quad (9)$$

IV. WELDING SEAM IDENTIFICATION

For a human being, it is very easy to find the welding seam profile from the polluted welding image; this is because a human being recognizes it in terms of its inherent structure without fully relying on the numerical measurement. It is very significant for a welding robot to extract and express the inherent structure of the welding seam profile like a human being. Our idea is inspired from the work [6], where the authors developed a syntactic method, but different from ours.[3]

A. Qualitative Description of the Welding Seam

For the welding seam profile without curve, they may be qualitatively described by utilizing line segment element $(L = \{l_i\}, i = 1, \ldots, N)$ and their junction relationship $(R = \{r_i(l_j, l_{j+1})\}, j = 1, \ldots, N - 1)$. As for the line segment element l_i, it may be jointly expressed by its length $length(l_i)$ and slope $slope(l_i)$. As for the junction r_i, there are two kinds of relationships, i.e., connection $(C = | c_j(l_j, l_{j+1}) |)$ and break $(G = | g_j(l_j, l_{i+1}) |)$, where c_j expresses the slope difference between two line segments connected. g_j may be regarded as one

---

[2]The Kalman filter is an algorithm that utilizes a series of measurements observed over time, containing statistical noise and other inaccuracies, and estimates some unknown variables that tend to be more precise than those based on a single measurement alone, by using Bayesian inference and estimating a joint probability distribution over the variables for each time frame.

[3]For example, the definitions of segment and junction relationship are different, i.e., first, in [6], the segment element was defined by only considering its length, instead of its length and slope together. Second, there were only three kinds of junction relationships defined. Third, the relationship element recovery was not considered and the syntactic rules used to organize the inherent structure is a bit complicated.

TABLE I
DEFINITION OF LINE SEGMENT ELEMENT

Qualitative description	Element	Symbol
Horizontal	⎯⎯	h
Vertical	│	v
Upswept	╱	u
Declivitous	╲	d

TABLE II
DEFINITION OF JUNCTION RELATIONSHIP ELEMENT

Qualitative description	Relationship	Symbol
Connection without the angle	⎯•⎯	c_1
Connection with the anticlockwise angle	╱•	c_2
Connection with the clockwise angle	⎯•╲	c_3
Horizontal break	⎯ ⎯	g_h
Vertical break	⎯⁝	g_v
Upswept break	⁖⎯	g_u
Declivitous break	⁖⎯	g_d

imaginary line segment, which also includes length and slope. Therefore, we can give a definition about line segment element and junction relationship in Tables I and II, respectively, so that there exists a mapping function $F = \rho(s)$ to describe the profile of joint/groove as character strings. For example, for a welding joint V, it can be qualitatively described as $\rho(s) = hc_3 dc_2 uc_3 h$.

Sometimes, the welding seam profile needs to be finer classified and matched, the line segment elements, i.e., upswept u and declivitous d in Table I, are refined by setting different thresholds T_e in terms of the slope. Similar to some junction relationships, i.e., upswept break g_u and declivitous break g_d, they may also be refined by setting different thresholds T_s.

B. Extraction of the Center Line of the Laser Stripe

After the Kalman filter, the laser stripe may be estimated in the rectangular window. Therefore, we only need to search and extract the center line of the laser stripe by scanning the gray column by column in the window according to (2).

Since disturbances of noise might lead to more than one wave peaks, a similarity measure is proposed to distinguish these peaks as

$$S_\alpha = \frac{W_w \left| f_w - f_w^c \right| + W_g \left| f_g - f_g^c \right|}{Max \left(\left| f_w - f_w^c \right|, \left| f_g - f_g^c \right| \right)} \quad (10)$$

where f_w and f_g are the maximum of width and gray of the standard laser stripe, respectively. f_w^c and f_g^c are the maximum of width and gray of the detecting laser stripe, respectively. W_w and W_g are the weights of width and gray of the laser stripe, $W_w + W_g = 1$. Obviously, $S_a \in [0,1]$ is a similarity measurement.[4] If

[4]It satisfies the definition of similarity [21], i.e., symmetry, consistency, and nonnegativity.

greater S_a is, and then, more the corresponding peak belongs to the laser stripe.

After the filtering of gray peaks, we can obtain the point set $P = \{p_i\}, i = 1, \ldots, M$, of the center line of the laser stripe. And then, they can be fitted to different segments utilizing the least-squares method [22].

C. Model-Based Matching

Welding seam recognition based on the model M is a method that can explain the image data of bottom layer via the top-layer model knowledge, i.e., element feature. If the profile is very ideal in the object image O_I, then the character string acquired from O_I will be fully consistent with the model M. As such, it is very simple to check their correspondence relationship. However, due to some interference factors, e.g., strong arc light, splashes, and reflections from the workpiece surface, and so on, the character string directly extracted from the physical welding image O_I is usual missing, repeated or irrelevant. In this case, how to find out this correspondence relationship is also our concern here.

1) Matching Hypothesis: Before matching, an evaluation to match or not between the model M and the object O_I needs to be conducted. Since the element features of a welding seam profile are strictly ordered from the left to right, a precondition is requested that the first element of the model M can be found to be the corresponding one in the object O_I, and the number of model character strings should be larger than those from the object O_I. Under this hypothesis, the matching position p between them must be remembered. If a matching does not hold, we can start a new assumption from position $p + 1$, in order to solve the problem that some foreign bodies are on the left, i.e., workholders.

2) Matching Testing: First, two definitions are given to explain the matching between the object O_I and the model M.

Definition 1: $\forall \{l_i\}_O, \{r_i\}_O, \in \{L, R\}_{O_I}$ and $\{l_j\}_M, \{r_j\}_M, \in \{L, R\}_M$, if $\exists < \{l_i\}_O, \{r_i\}_O, \{l_{i+1}\}_O > \equiv < \{l_j\}_M, \{r_j\}_M, \{l_{j+1}\}_M >$, then $< \{l_i\}_{M \to O}, \{r_i\}_{M \to O}, \{l_{i+1}\}_{M \to O} >$ is called as TGM, i.e., triple group matching, where the symbol "$\equiv$" expresses fully consistent.

When $\{l_1\}\{r_1\}\{l_2\}, \ldots, \{l_i\}\{r_i\}\{l_{i+1}\}, \ldots, \{l_M\}$ from the model M are searched to match in the object O_I, we adopt the TGM $< \{l_i\}_{M \to O}, \{r_i\}_{M \to O}, \{l_{i+1}\}_{M \to O} >$ in sequence.

Definition 2: If $\forall < \{l_i\}_O, \{r_i\}_O, \{l_{i+1}\}_O >$, and always $\exists < \{l_j\}_M, \{r_j\}_M, \{l_{j+1}\}_M >$ is matched with it on the exact position index j, i.e., $< \{l_j\}_{M \to O}, \{r_j\}_{M \to O}, \{l_{j+1}\}_{M \to O} >$, moreover, the tripe matching items of $< \{l_{i+1}\}_O, \{r_{i+1}\}_O, \{l_{i+2}\}_O >$ can only be found at the index $j + 1$, Therefore, we call the matching way as STGM, i.e., sequence triple group matching.

After STGM, the object O_I may be matched with the model M. Since both the object O_I and the model M are qualitatively described as character strings, i.e., $\{l_1\}\{r_1\}\{l_2\}, \ldots, \{l_i\}\{r_i\}\{l_{i+1}\}, \ldots, \{l_N\} \in \{L, R\}_{O_I} \Rightarrow \{s_1, s_2, s_3, \ldots, s_N\} \in S_O$ and $\{l_1\}\{r_1\}\{l_2\}, \ldots, \{l_i\}\{r_i\}\{l_{i+1}\}, \ldots, \{l_M\} \in \{L, R\}_M \Rightarrow \{s_1, s_2, s_3, \ldots, s_M\} \in S_M$. The STGM matching step is performed between S_O and S_M. Here, we choose TGM, instead of sequence element matching
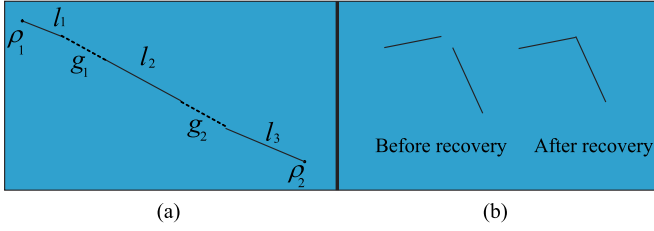
Fig. 5. (a) Multiple-segment element integration and (b) relationship element recovery.

one by one, which can assure the recovery of the element relationship between the former and latter two elements according to the model M, when the acquired element relationship $\{r_i\}$ is incorrect. Before the qualitative matching algorithm is given, two concepts, i.e., segment element integration and relationship element recovery, are defined as follows:

a) *Segment element integration:* If a segment element of the model has the corresponding n continuous segment elements found in an object O_I, which might be broken by some disturbances, i.e., splashes, etc., then they can be integrated into one big segment element. In order to do that, we need to compute their degree of collinearity, which is defined as

$$D_c = Dis(\rho_1, \rho_2) / \left[\sum_{i=1}^{n} L(l_i) + \sum_{j=1}^{n-1} L(g_j) \right] \qquad (11)$$

where ρ_1 and ρ_2 are, respectively, expressed as the initial point of segment element l_1 and the end point of segment element l_3 in Fig. 5(a). $Dis(\rho_1, \rho_2)$ represents the distance[5] between two points, i.e., ρ_1 and ρ_2. $L(\cdot)$ represents the length of segment. If the degree of collinearity $D_c > T_c$, then these segment elements can be integrated, where T_c is a threshold of degree of collinearity.

b) *Relationship element recovery:* Due to the disturbances, some junction relationships acquired from the object O_I, i.e., connection (c_1, c_2, c_3) and break (g_h, g_v, g_u, g_d) in Table II, might change and even be conflictive with the original model. For example, a relationship obtained from O_I is a break after the fitting processing between two segments, as shown in Fig. 5(b). However, we know that, actually, it is a kind of connection c_3 from the model. Although we have obtained the other two matching items from the TGM way, since c_3 does not match the break, the object O_I does yet not match the model M, so that a mistaken conclusion is reached. Therefore, the relationship element recovery proposed here is very necessary in the process of search matching, which must satisfy the following conditions:

1) $\{l_i\}_O \bowtie \{l_{i+1}\}_O, \{l_i\}_O, \{l_{i+1}\}_O \in O_I$;
2) $\{l_i\}_M \bowtie \{l_{i+1}\}_M, \{l_i\}_M, \{l_{i+1}\}_M \in M$;
3) $\{l_i\}_{M \to O} \bigcap \{l_{i+1}\}_{M \to O}, i \in N$;
4) $\{R_i\}_O \neq \{R_i\}_M$;

where $\bowtie$ represents the relationship of *adjacent*. $\bigcap$ represents the relationship of *and*.

Algorithm 2: Algorithm of search matching.

Input: $\exists \{l_j\}_O, \{r_j(l_j, l_{j+1})\}_O, \{l_{j+1}\}_O, j \in \Im$ in an object image O_I
Output: $\{l\}_{M \to O}, \{r(\cdot)\}_{M \to O}$
1 **for** $i \to 1; i \leq \Re$ **do**
2    $\forall \{l_i\}_M, \{r_i(l_i, l_{i+1})\}_M, \{l_{i+1}\}_M, i \in \Re$ from a model;
3   **for** $j \to 1; j \leq \Im$ *and* $k \to 1; k \leq \Im - j$ **do**
4   Search the matching item $\{l_j\}_O$ of $\{l_i\}_M$ in object O_I and remember its position k.;
5   **while** *not end of* k **do**
6   Search the matching item $\{l_\phi\}_O, \phi > k$ of $\{l_{i+1}\}_M$ from position $k + 1$;
7   **if** $\exists$ *multiple segment elements* $\{l_\varphi\}_O, \varphi \in [j, \phi]$ **then**
8   **if** *The degree of collinearity in (11)* $D_c > D_c^t$
9   *//Here D_c^t refers to the threshold of degree of collinearity* **then**
10   Integrate these segment elements $\{l_\varphi\}_O$;
11   **if** $\{r_i(l_j, l_\phi)\}_O \neq \{r_i(l_i, l_{i+1})\}_M$ *and satisfies the condition of recovery of relationship element*
12   **then**
13   Recover the relationship element $\{r_i(l_j, l_\phi)\}_O$ in terms of $\{r_i(l_i, l_{i+1})\}_M$
14   **return** $\{l_i\}_{M \to O}, \{r_i(l_i, l_{i+1})\}_{M \to O}, \{l_{i+1}\}_{M \to O}$;
15 **return** $\{l\}_{M \to O}, \{r(\cdot)\}_{M \to O}$;

For example, a break[6] between two segments before recovery in Fig. 5(b), according to the model, as we know, it is a c_3 junction, and then, we can extend the two segment element, respectively, until they intersect. Therefore, the c_3 junction is recovered.

3) Search Matching

When we begin to search the marching between the model M and the object O_I, the TGM method is utilized. However, since there are some uncertainties about the feature segments extracted in terms of the least-squares method, when some disturbances turn up, i.e., one segment is separated into two or several ones, which are similar or close, but are not collinear as shown in Fig. 5(a), or a break occurs between two neighboring segments as shown in Fig. 5(b), segment element integration or/and relationship element recovery is/are needed in the process of search matching. Therefore, the search matching algorithm to find the corresponding matching item $\{r_i(l_i, l_{i+1})\}_{M \to O}$ from the object O_I is given in algorithm 2.

D. Welding Seam Position

If the matching is performed well between the object O_I and the model M, the welding seam can be well identified. Although we have already known what type the welding seam is at this time, we do not know where the welding seam is. How to define a position to be followed by robot is very important for

---

[5]Here, the Euclidean distance is used; of course, readers may also choose others.

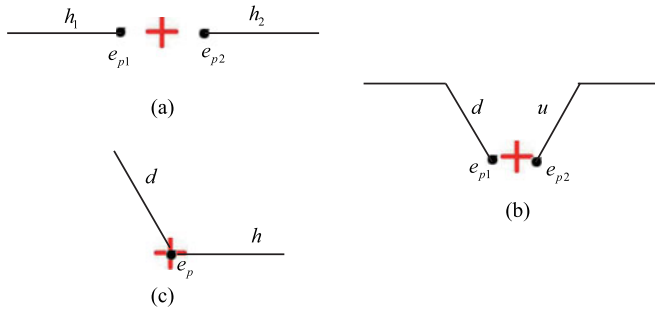[6]There is a straight line segment supposed between the gap.

Fig. 6. Definition of welding seam position. (a) Butt joint for the I groove. (b) Butt joint for the V groove. (c) Angle welding.

TABLE III
PERFORMANCE PARAMETER OF THE STRUCTURED-LIGHT SENSOR

AM (°)	HM (mm)	FOV (mm × mm)	RM (mm × mm)	DF (mm)
22.235	122	65× 155	0.1× 0.25	25

(Note: **AM** refers to the angle of measurement; **HM** refers to the height of measurement; **FOV** refers to the field of vision; **RM** refers to the resolution of measurement; **DF** refers to the depth of field).

automatic welding. The position is defined in terms of different joints/grooves,[7] which are partially enumerated in Fig. 6.

1) For the butt joint for **I** groove as shown in Fig. 6(a), first, find the top edge segment elements, i.e., h_1 and h_2, of the groove and then pick up the right end point e_{p1} and left end point e_{p2}. Finally, the midpoint calculated between e_{p1} and e_{p2} is regarded as the position of **I** groove welding seam.

2) For the butt joint for the **V** groove with gap as shown in Fig. 6(b), first, find the declivitous segment element d and upswept element u of the groove and then pick up the right end point e_{p1} and left end point e_{p2}. Finally, the midpoint calculated between e_{p1} and e_{p2} is regarded as the position of welding seam **V** groove with gap.

3) For angle welding as shown in Fig. 6(c), first, find the declivitous segment element d and upswept element u or horizontal upswept element h of the groove, and since d and u or h intersect at the position e_p, it is regarded as the position of the angle welding seam.

V. EXPERIMENTS

This experiment is performed by industrial robot $KR16$ developed by KUKA, a well-known German robot company, on which the TBI welding gun[8] is fixed. The welding machine EWM PHOENIX 400 is adopted, which is fit for MIG/MAG/TIG welding. Shielding gas used here is composed of $AR(80\%)+CO_2(20\%)$. The structured-light sensor with 58 frames/s sampling rate (its performance parameter is given in Table III) is utilized to acquire the information of welding

[7]Here only include several special kinds of joints/grooves without the curve segment elements.
[8]produced by German TBi Industries GmbH.
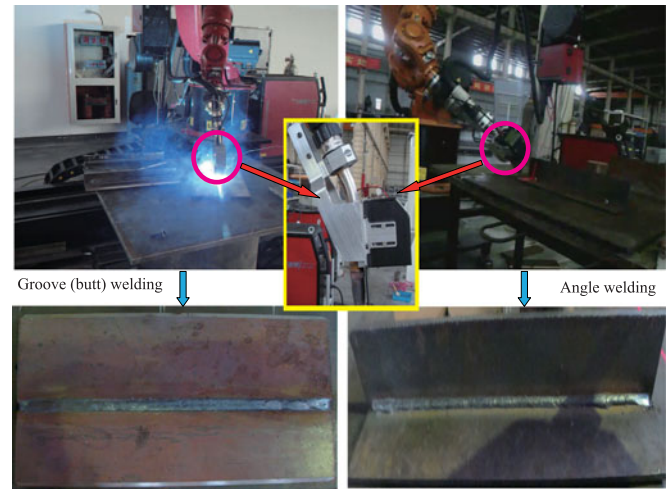
Fig. 7. Welding experiment environment and welding workpieces.
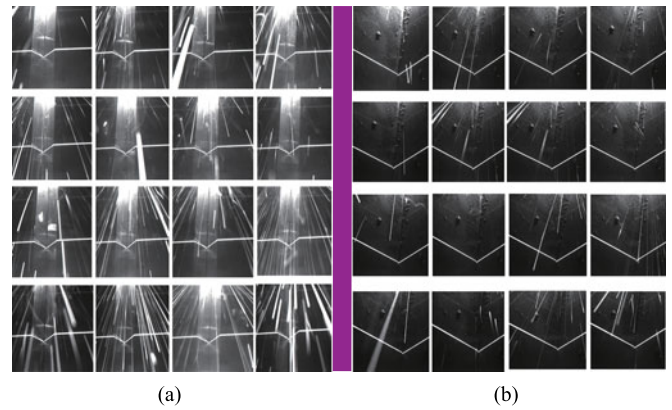
Fig. 8. Parts of (a) V groove welding and (b) angle welding images.
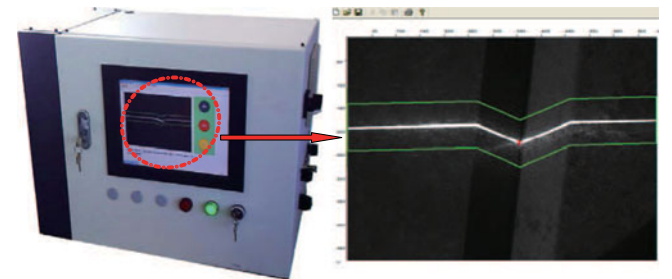
Fig. 9. Vision processor.

joint/groove, which is installed at the end of effector of $KR16$. In this experiments, the new algorithm is testified on two kinds of welding types, i.e., V groove welding (welding workpieces are composed of two 450-mm-long and 10-mm-thick carbon steels(45#), on which there is a straight butt welding seam with 90° V groove and 3-mm truncated edge) and angle welding (welding workpieces are composed of two 400-mm-long and 10-mm-thick carbon steels (45#), between which the angle is 90°), as shown in Fig. 7. The obtained images[9] including

[9]Here, the image size is 640 × 480 pixels.

Fig. 10. Communication between the vision processor and the robot controller.

110 pieces of V types of welding images and 72 pieces of angle welding images are partially shown in Fig. 8, respectively, which are processed on a vision processor,[10] as shown in Fig. 9. The parameters of the Kalman filter is given in the following:

$$A = \begin{bmatrix} 1 & 0 & 1 & 0 \\ 0 & 1 & 0 & 1 \\ 0 & 0 & 1 & 0 \\ 0 & 0 & 0 & 1 \end{bmatrix}, \quad P = \begin{bmatrix} 10 & 0 & 0 & 0 \\ 0 & 10 & 0 & 0 \\ 0 & 0 & 10 & 0 \\ 0 & 0 & 0 & 10 \end{bmatrix}$$

$$H = \begin{bmatrix} 1 & 0 & 0 & 0 \\ 0 & 1 & 0 & 0 \end{bmatrix}, \quad R = \begin{bmatrix} 0.2845 & 0.0045 \\ 0.0045 & 0.0455 \end{bmatrix}$$

$$Q = \begin{bmatrix} 0.01 & 0 & 0 & 0 \\ 0 & 0.01 & 0 & 0 \\ 0 & 0 & 0.01 & 0 \\ 0 & 0 & 0 & 0.01 \end{bmatrix}$$

where we suppose that W_k is the Gaussian white noise with variance Q[11]

Generally speaking, mean absolute error (*i.e.*, *Mae*) is used to evaluate the static precision of the system, standard deviation/variation (*i.e.*, *Var*) is used to evaluate the stability/robustness of the system, and error is used to evaluate the dynamic precision of the system.

A. Effect of the Search Window Size

There are two experiments conducted for two types of welding seams, respectively, i.e., V-type groove and angle welding seam. For the initial window size of whatever of them, the window justly contains the laser stripe. In Fig. 11, the static precision (*Mae*) and stability of system (*Var*) are testified when 110 frames of welding images with the V groove are, respectively, fed with the increment of the search window size toward up and down two directions simultaneously. As seen from Fig. 11, we find that *Var* in the X-direction is low near 2.8 at the beginning of size increment, and then is falling gradually, when

Fig. 11. Effect of the window size on the V-type groove.

Fig. 12. Effect of the window size on the angle welding seam.

the size is enlarged to 10 pixels nearby, its *Var* drops down sharply, then rises sharply to 3.3, and then drops down a bit and keeps constant for going to increase the window size ever since. However, as seen from Fig. 12, for the angle welding seam, when 72 frames of welding images are fed, respectively, its *Var* is very low at the beginning of size increase of the search window, and then, with the increment of size, its *Var* increases gradually. For the Y-direction, whatever for the V-type groove or the angle welding seam, the change of *Var* looks very similar to that in the X-direction except low rangeability. However, the *Mae* for the V-type groove in the X-direction is very high at the beginning of the size increase from Fig. 11 and, then, reduces rapidly and fluctuates lightly with the increase of window size. Until 1.37 nearby, the *Mae* almost keeps constant when going to increase the window size from 30 pixels. While in the Y-direction, the *Mae* is low at the beginning of size increment, and with the increase of size, it has a small fluctuation. Finally, until 0.84, the *Mae* also almost keeps constant when going to increase the window size from 30 pixels. For the angle welding seam in Fig. 12, whatever in the X- or Y-direction, the *Mae* is

TABLE IV
EFFECT OF IMAGE PREPROCESSING ON THE V GROOVE

	Mae X	*Var* X	*Mae* Y	*Var* Y
C_1	1.4085	5.1654	0.7183	0.6926
C_2	1.1549	2.6821	0.6901	0.5497
C_3	1.1549	2.8245	0.6761	0.5247
C_4	1.0986	2.6245	0.6761	0.5247

Note: C_1 represents the result without filter preprocessing; C_2 represents the result with a 5×5 median filter; C_3 represents the result with a column median filter; C_4 represents the result after C_2 and C_3.

TABLE V
EFFECT OF IMAGE PREPROCESSING ON THE ANGLE WELDING SEAM

	Mae X	*Var* X	*Mae* Y	*Var* Y
C_1	1.2752	2.4949	0.7339	0.7554
C_2	1.2018	2.2251	0.7156	0.6855
C_3	1.2294	2.3581	0.6972	0.6706
C_4	1.1835	2.1755	0.6972	0.6706

TABLE VI
COMPARISON ON THE V GROOVE

	Mae X	*Var* X	*Mae* Y	*Var* Y	time(s)
Δ_1	1.4366	9.1300	0.8451	1.7517	0.0596
Δ_2	1.3003	5.3541	0.7020	1.2788	0.0362
Δ_3	2.1025	15.1284	0.9583	2.8818	0.0443
Δ_4	2.5925	22.5237	1.5034	6.2445	0.0603
Δ_5	3.0792	33.3857	1.7781	8.8511	0.0529
Δ_6	1.0986	2.6245	0.6761	0.5247	0.0545

Note: Δ_1 represents the result without the Kalman filter; Δ_2 represents the result with the method in [16]; Δ_3 represents the result with the method [17]; Δ_4 represents the result with the method in [6]; Δ_5 represents the result with the method in [23]; Δ_6 represents the result with ours proposed here.

TABLE VII
COMPARISON ON ANGLE WELDING

	Mae X	*Var* X	*Mae* Y	*Var* Y	time(s)
Δ_1	4.0301	8.9845	1.3025	3.6051	0.0587
Δ_2	1.4488	4.0524	0.7441	1.7352	0.0384
Δ_3	1.8115	6.6189	1.1378	4.2633	0.0431
Δ_4	2.4478	12.4079	1.3556	5.4169	0.0583
Δ_5	3.1946	20.2931	1.7475	8.0567	0.0514
Δ_6	1.1835	2.1755	0.6972	0.6706	0.0532

very low at the beginning and also fluctuates a bit with the increase of size, but there is a global rising tendency. For the *Mae* in the X-direction, it rapidly increases and reaches 12 nearby and, then, becomes gentle and even drops a bit with the enlargement of window. For the *Mae* in the Y-direction, it gradually increases and reaches 4 nearby; of course, there are some small fluctuations in this course of size increment. Through the comprehensive analysis on these experiment results, the window size should be enlarged to 3 pixels from the initial size toward up and down two directions, where the search window almost plays the best performance in static precision and stability of the system.

B. Effect of Image Preprocessing

In order to evaluate the effect of image preprocessing on the static precision and stability of the system, 110 frames of welding images with the V groove and 72 frames with the angle welding seam are, respectively, fed to compute their *Mae* and *Var*, when the search window size is set at 3 pixels from the initial size toward up and down two directions. The experiment result for the V groove is given in Table IV and the one for the angle welding seam is given in Table V, where it obviously shows that the image preprocessing step plays an important role in improving the static precision and stability of the system, since C_4 has the minimum value about *Mae* and *Var* in the X- and Y-directions.

C. Comparison With Other Methods in Precision, Stability, and Real Time

Here, we also compare our method Δ_6 proposed here with other methods [6], [16], [17], [23] in precision, stability, and real time of the system. Of course, in order to embody the

advantage of using the Kalman filter, the method without the Kalman filter Δ_1 is also compared with Δ_6. Similarly, 110 frames of welding images with the V groove and 72 frames with the angle welding seam are, respectively, input to testify the performance of every method, i.e., static precision, stability, and real time.

The experiment results are given in Table VI for the V groove and in Table VII for the angle welding seam. Obviously, our method has the highest static precision and stability among all methods, i.e., $\Delta_1 \sim \Delta_5$; however, its real-time performance has a discount and is not the best one, which lies in the midst of them. Moreover, we find that the processing time of every frame with Δ_6 is very close to that with Δ_1, although the search window with the Kalman filter is able to reduce the search space, since it also spends a certain amount of time in the running of the Kalman filter itself.

D. Comparison With Other Methods in Dynamic Precision

Here, we also compare our method Δ_6 proposed here with other methods [6], [16], [17], [23] in dynamic precision. When 110 frames of welding images with V groove and 72 frames with angle welding seam are respectively and sequentially processed to calculate the error between the measurement value and actual value in the X- and Y-directions. The experiment results are shown in Fig. 13, where our method Δ_6 has the highest dynamic precision for whatever V groove or angle welding seam with the sequential frames fed, since its fluctuation range $[-3, 3]$ is the smallest one.
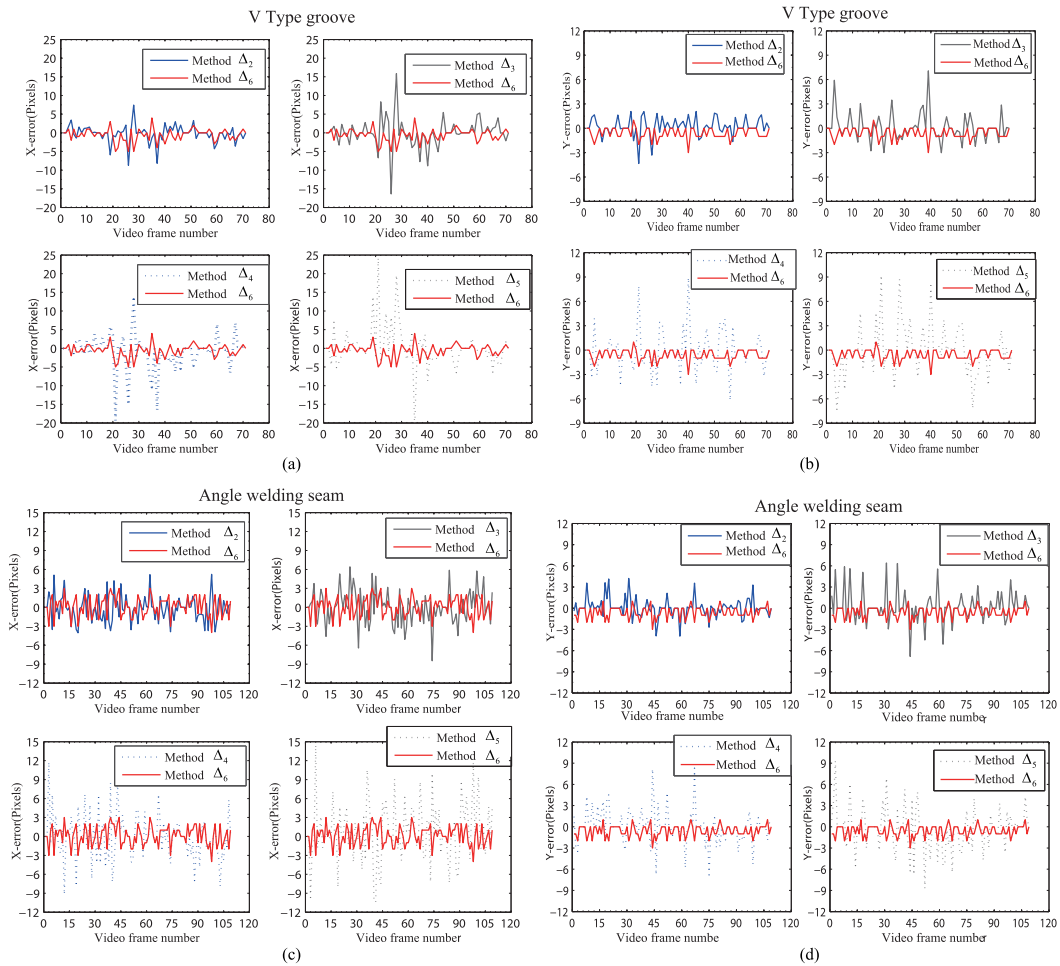
Fig. 13. Comparison of dynamic precision. (a) Synamic precision in the X-direction for the V-type groove. (b) Dynamic precision in the Y-direction for the V-type groove. (c) Dynamic precision in the X-direction for the angle welding seam. (d) Dynamic precision in the Y-direction for the angle welding seam.

VI. CONCLUSION

With the aim to avoid the disturbances, i.e., strong arc lights, welding splashes, misalignments/malpositions, thermal-induced deformations, welding fumes, and to improve the welding position precision and stability, a robust automatic welding seam identification and tracking method for mid/thick plates was proposed in this paper, novelties of which include: first, the Kalman filter was adopted to track the laser stripe in order to limit the range of searching the profile of the welding seam; second, in order to improve the recognition precision and robustness, a character string method was used to qualitatively describe the profile of the welding seam. Some experiments were performed, i.e., the effect of the search window, the effect of image preprocessing, the comparison with other methods in static precision, stability, and real-time and dynamic precision, to testify our method proposed here, which keeps real-time, has the distinct preponderance over other methods in static and dynamic precision and stability, although its real-time performance is not the best among all the methods. However, currently, our method is yet not fit for the curve profile of welding seam, i.e., U groove and so on, since the qualitative description on the curve profile is not proposed here, which is our next research focus.

In addition, the control precision of robot [24], [25] is not considered in the current work, which will be integrated into our future work.

REFERENCES

[1] D. Y. You, X. D. Gao, and S. Katayama, "WPD-PCA-based laser welding process monitoring and defects diagnosis by using FNN and SVM," *IEEE Trans. Ind. Electron.*, vol. 62, no. 1, pp. 628–636, Apr. 2015.

[2] X. D. Gao, D. Y. You, and S. Katayama, "Seam tracking monitoring based on adaptive Kalman filter embedded Elman neural network during high-power fiber laser welding," *IEEE Trans. Ind. Electron.*, vol. 59, no. 11, pp. 4315–4325, Apr. 2012.

[3] Z. Z. Wang, "An imaging and measurement system for robust reconstruction of weld pool during arc welding," *IEEE Trans. Ind. Electron.*, vol. 62, no. 8, pp. 5109–5118, Feb. 2015.

[4] J. Wu, J. S. Smith, and J. Lucas, "Weld bead placement system for multipass welding," *Proc. Inst. Elect. Eng.—Sci., Meas., Technol.*, vol. 143, no. 2, pp. 85–90, Mar. 1996.

[5] Y. Li, D. Xu, Y. Shen, and M. Tan, "Multi-features selection and extraction of structured light images of vision sensor for seam tracking," *Chin. J. Sens., Actuators*, vol. 19, no. 6, pp. 2676–2681, Dec. 2006.

[6] P. Sicard and M. D. Levine, "Joint recognition and tracking for robotic arc welding," *IEEE Trans. Syst. Sci. Cybern.*, vol. 19, no. 4, pp. 714–728, Aug. 1989.

[7] M. Dinham and G. Fang, "Detection of fillet weld joints using an adaptive line growing algorithm for robotic arc welding," *Robot., Comput. Integr. Manuf.*, vol. 30, no. 3, pp. 229–243, Nov. 2014.
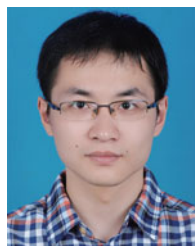
[8] M. Dinham and G. Fang, "Autonomous weld seam identification and localisation using eye-in-hand stereo vision for robotic arc welding," *Robot., Comput. Integr. Manuf.*, vol. 29, no. 5, pp. 288–301, Oct. 2013.

[9] M. A. Fischler and R. C. Bolles, "Random sample consensus: A paradigm for model fitting with applications to image analysis and automated cartography," *Commun. ACM*, vol. 24, no. 6, pp. 381–395, Jun. 1981.

[10] Y. L. Xiong, F. H. Shi, T. Lin, and S. B. Chen, "Efficient weld seam detection for robotic welding based on local image processing," *Ind. Robot, Int. J.*, vol. 36, no. 3, pp. 277–283, Jun. 2009.

[11] Y. S. He, Y. X. Chen, Y. L. Xu, Y. M. Huang, and S. B. Chen, "Autonomous detection of weld seam profiles via a model of saliency-based visual attention for robotic arc welding," *J. Intell. Robot Syst.*, vol. 81, no. 3-4, pp. 395–406, Mar. 2016.

[12] B. Chen and J. C. Feng, "Multisensor information fusion of pulsed GTAW based on improved DS evidence theory," *J. Int. J. Adv. Manuf. Technol.*, vol. 71, nos. 1–4, pp. 91–99, Nov. 2014.

[13] G. Shafer, *A Mathematical Theory of Evidence*, vol. 1, 1st ed. Princeton, NJ, USA: Princeton Univ. Press, Apr. 1976.

[14] D. Y. You, X. D. Gao, and S. Katayama, "Multisensor fusion system for monitoring high-power disk laser welding using support vector machine," *IEEE Trans. Ind. Informat.*, vol. 10, no. 2, pp. 1285–1295, Mar. 2014.

[15] W. H. Li, K. Gao, J. Wu, T. Hu, and J. Y. Wang, "SVM-based information fusion for weld deviation extraction and weld groove state identification in rotating arc narrow gap mag welding," *Int. J. Adv. Manuf. Technol.*, vol. 74, nos. 9–12, pp. 1355–1364, Jun. 2014.

[16] H. Y. Chen, W. P. Liu, L. Y. Huang, G. S. Xing, M. Wang, and H. X. Sun, "The decoupling visual feature extraction of dynamic three-dimensional v-type seam for gantry welding robot," *Int. J. Adv. Manuf. Technol.*, vol. 80, nos. 9–12, pp. 1741–1749, Apr. 2015.

[17] Q. Q. Wu *et al.*, "A study on the modified hough algorithm for image processing in weld seam tracking," *J. Mech. Sci. Technol.*, vol. 29, no. 11, pp. 4859–4865, Dec. 2015.

[18] C. Umeagukwu and J. McCormick, "Investigation of an array technique for robotic seam tracking of weld joints," *IEEE Trans. Ind. Electron.*, vol. 38, no. 3, pp. 223–229, Aug. 1991.

[19] R. E. Kalman, "A new approach to linear filtering and prediction problems," *J. Basic Eng.*, vol. 82, no. 1, pp. 35–45, Mar. 1960.

[20] K. Haug and G. Pritschow, "Robust laser-stripe sensor for automated weld-seam-tracking in the shipbuilding industry," in *Proc. 24th Annu. Conf. IEEE Ind. Electron. Soc.*, Aug. 1998, vol. 2, pp. 1236–1241.

[21] X. D. Li, J. Dezert, F. Smarandache, and X. Huang, "Evidence supporting measure of similarity for reducing the complexity in information fusion," *Inf. Sci.*, vol. 181, no. 10, pp. 1818–1835, May 2011.

[22] S. M. Stigler, "Gauss and the invention of least squares," *Ann. Statist.*, vol. 9, pp. 465–474, May 1981.

[23] J. Aviles-Viñas, I. Lopez-Juarez, and R. Rios-Cabrera, "Acquisition of welding skills in industrial robots," *Ind. Robot, Int. J.*, vol. 42, no. 2, pp. 156–166, Apr. 2015.

[24] M. Van, S. S. Ge, and H. L. Ren, "Finite time fault tolerant control for robot manipulators using time delay estimation and continuous nonsingular fast terminal sliding mode control," *IEEE Trans. Cybern.*, doi: 10.1109/TCYB.2016.2555307.

[25] M. Van, S. S. Ge, and H. L. Ren, "Robust fault-tolerant control for a class of second-order nonlinear systems using an adaptive third-order sliding mode control," *IEEE Trans. Syst., Man, Cybern., Syst.*, vol. 47, no. 2, pp. 221–228, Jun. 2017.

Xianghui Li was born in Yancheng, China, in 1992. He received the B.Sc. degree in automation in 2014 from Southeast University, Nanjing, China, where he is currently working toward the Ph.D. degree in pattern recognition.

His research interests include deep learning and place identification.

Mr. Li received the Second Prize in the National Mathematical Modeling Contest in 2015.

Shuzhi Sam Ge (S'90–M'92–SM'99–F'06) received the B.Sc. and M.Sc. degrees in control engineering from Beijing University of Aeronautics and Astronautics, Beijing, China, in 1986 and 1988, respectively, and the Ph.D. degree in mechanical/electrical engineering from the Imperial College of Science, Technology and Medicine, University of London, London, U.K., in 1993.

He is the Founding Director of the Robotics Institute and the Institute of Intelligent Systems and Information Technology, University of Electronic Science and Technology of China, Chengdu, China. He is also the Founding Director of the Social Robotics Laboratory, Interactive Digital Media Institute, National University of Singapore, Singapore, where he is currently a Professor in the Department of Electrical and Computer Engineering.

Prof. Ge is the Editor-in-Chief of the *International Journal of Social Robotics*. He has served as an Associate Editor for a number of flagship journals. He has also served as the Vice-President of Technical Activities from 2009 to 2010 and of Membership Activities from 2011 to 2012 for the IEEE Control Systems Society.

Mohammad Omar Khyam received the B.Sc. degree in electronics and telecommunication engineering from Rajshahi University of Engineering and Technology, Rajshahi, Bangladesh, in 2010, and the Ph.D. degree in electrical engineering from the University of New South Wales, Kensington, Australia, in 2015.

He is currently a Postdoctoral Research Fellow with the National University of Singapore, Singapore. His research interests include signal processing and wireless communication.

Xinde Li (M'09–SM'16) received the Ph.D. degree in control theory and control engineering from the Department of Control Science and Engineering, Huazhong University of Science and Technology, Wuhan, China, in 2007.

After receiving the Ph.D. degree, he joined the School of Automation, Southeast University, Nanjing, China, where he is currently a Professor and a Ph.D. Supervisor. From 2012 to 2013, he was a Visiting Scholar with the School of Interactive Computing, Georgia Institute of Technology. In 2016, he was a Postdoctoral Research Fellow with the Department of Electrical and Computer Engineering, National University of Singapore. His research interests include information fusion, object recognition, computer vision, intelligent robots, and human–robot interaction.

Prof. Li received a Talent of Qing Lan Project Award of Jiangsu Province and a Six Major Top-talent Plan Award of Jiangsu Province, China.

Chaomin Luo (S'01–M'08) received the B.Eng. degree in electrical engineering from Southeast University, Nanjing, China, the M.Sc. degree in engineering systems and computing from the University of Guelph, Guelph, ON, Canada, and the Ph.D. degree in electrical and computer engineering from the University of Waterloo, Waterloo, ON, Canada, in 2008.

He is currently an Associate Professor with the Department of Electrical and Computer Engineering, University of Detroit Mercy, Detroit, MI, USA. His research interests include robotics and automation, control and intelligent systems, mechatronics, embedded systems, and very large scale integrated design automation.

Dr. Luo received the Postgraduate Scholarship from the Natural Sciences and Engineering Research Council of Canada.